Simultaneous Acquisition of Spatial Harmonics (SMASH): Fast Imaging with Radiofrequency Coil Arrays

Daniel K. Sodickson, Warren J. Manning

SiMultaneous Acquisition of Spatial Harmonics (SMASH) is a new fast-imaging technique that increases MR image acquisition speed by an integer factor over existing fast-imaging methods, without significant sacrifices in spatial resolution or signal-to-noise ratio. Image acquisition time is reduced by exploiting spatial information inherent in the geometry of a surface coil array to substitute for some of the phase encoding usually produced by magnetic field gradients. This allows for partially parallel image acquisitions using many of the existing fast-imaging sequences. Unlike the data combination algorithms of prior proposals for parallel imaging, SMASH reconstruction involves a small set of MR signal combinations prior to Fourier transformation, which can be advantageous for artifact handling and practical implementation. A twofold savings in image acquisition time is demonstrated here using commercial phased array coils on two different MR-imaging systems. Larger time savings factors can be expected for appropriate coil designs.

Key words: fast imaging; RF coil array; simultaneous acquisition; MR image reconstruction.

INTRODUCTION

The speed with which magnetic resonance images may be acquired has increased dramatically over the past decade. The improvements in speed may be traced to a combination of advances in technology and innovations in imaging strategy. Strong, fast-switching magnetic field gradients and fast electronics have allowed the intervals between data collections to be reduced significantly. Meanwhile, fast gradient-echo and spin-echo sequences have reduced image acquisition time by allowing greater portions of k-space to be sampled after each spin excitation. For example, echo-planar imaging (EPI) (1), fast low-angle shot (FLASH) (2), turbo spin echo (TSE) (3), spiral imaging (4, 5), and BURST (6, 7) sequences all allow very short intervals between acquisition of successive data points. One common feature of these fast imaging techniques, however, is that they all acquire data in a sequential fashion. Whether the k-space data matrix is filled in a rectangular raster pattern, a spiral pattern, a rapid series of line scans, or some other novel trajectory, it is always acquired one point and one line at a time.

This report presents a fast-imaging technique that allows some fraction of signal data points to be acquired *in parallel*, rather than sequentially in time. Previously, several fast imaging schemes have been proposed using simultaneous data acquisition in multiple RF coils (8–13). The technique described here, dubbed simultaneous acquisition of spatial harmonics (SMASH), reduces image acquisition times by a multiplicative integer factor without a significant sacrifice in spatial resolution or signal-to-noise ratio (SNR), in effect by scanning many lines of k-space at a time. The SMASH procedure operates by using linear combinations of simultaneously acquired signals from multiple surface coils with different spatial sensitivities to generate multiple data sets with distinct offsets in k-space. The full k-space matrix may then be generated with only a fraction of the usual number of phase-encoding gradient steps. Consequently, the total image acquisition time may be reduced by the same fraction. A factor of two time savings has been implemented with standard equipment, although in principle, there is no limit to the number of lines that may be scanned simultaneously, provided coil arrays with sufficient numbers of components are constructed. Importantly, the SMASH technique may be combined with most existing fast-imaging sequences, thereby multiplying the intrinsic speed of these sequences.

THEORY

Phase Encoding by Amplitude Modulation

In the general case, the MR signal for a plane with spin density $\rho(x, y)$ and receiver coil sensitivity $C(x, y)$ may be written as

$$S(k_x, k_y) = \int\int dx\,dy\,C(x, y)\rho(x, y)\exp\{-ik_x x - ik_y y\} \quad [1]$$

where $k_x = \gamma G_x t_x$ and $k_y = \gamma G_y t_y$ as usual, with γ the gyromagnetic ratio, G_x and G_y the magnitude of the x and y gradients, and t_x and t_y the times spent in the x and y gradients, respectively. Here, the spin excitation function as well as the effects of relaxation have been incorporated into the pulse-sequence-specific sensitivity function C. For regions of the sample in which the coil sensitivity is relatively homogeneous, $C(x, y) \approx 1$, and $S(k_x, k_y)$ is then equal to the spatial Fourier transform of the spin-density function. Inverse Fourier transformation with respect to k_x and k_y reconstructs the usual spin-density image $\rho(x, y)$.

It is well known that MR receiver coils, especially surface coils, do not have uniform sensitivity. Signals from different regions of the imaged volume produce different currents in an RF coil, with the spatial variation

in sensitivity being simply related to the inhomogeneity of RF field produced by the coil over the sample volume. For a standard circular surface coil, there is a monotonic fall-off of sensitivity with distance from the coil in all directions.

If instead of a standard surface coil we construct an arrangement of surface coils with *sinusoidal* spatial sensitivity profiles, the MR signal from these coils will have an information content somewhat different from that of the usual coil signal. From the point of view of the theory, it does not matter whether the coils in question are singular coils with intrinsic sinusoidal sensitivities or whether they are composites of multiple smaller coils, whose signals are combined to produce the desired sinusoidal sensitivity profiles. In either case, appropriate combinations of coil outputs may be configured to have a composite sensitivity in the form of a complex exponential function: For example, complex combination of a cosinusoidal and a sinusoidal sensitivity with the same wavelength $\lambda_y^{\mathrm{comp}} = 2\pi/\Delta k_y^{\mathrm{comp}}$ yields a composite sensitivity of the form

$$C^{\mathrm{comp}}(x, y)$$

$$= \cos \Delta k_y^{\mathrm{comp}} y + i \sin \Delta k_y^{\mathrm{comp}} y = \exp\{i \Delta k_y^{\mathrm{comp}} y\}, \quad [2]$$

Here, $\Delta k_y^{\mathrm{comp}}$ denotes the spatial frequency of the composite complex exponential sensitivity.

Combining Eqs. [1] and [2] yields the following expression for the MR signal

$$S(k_x, k_y)$$

$$= \iint dx dy \rho(x, y) \exp\{-ik_x x - i(k_y - \Delta k_y^{\mathrm{comp}})y\} \quad [3]$$

$$= \hat{\rho}(k_x, k_y - \Delta k_y^{\mathrm{comp}})$$

where the ^ operator indicates a spatial Fourier transform. In other words, the combined MR signal from the inhomogeneous coils is shifted in k-space by an amount $(-\Delta k_y^{\mathrm{comp}})$. This k-space shift has precisely the same form as the shift produced by evolution in a y gradient of magnitude $\gamma G_y t_y = -\Delta k_y^{\mathrm{comp}}$. It appears, therefore, that appropriate modulations in the *amplitude* of the spatially varying sensitivity function can be used to take the place of phase or frequency encoding normally produced by magnetic field gradients.

Spatial Harmonic Generation Using RF Coil Arrays

In its simplest implementation, the SMASH technique uses a linear array of surface coils to synthesize multiple sinusoidal sensitivity variations. This procedure is compatible with traditional phased array coil designs. As mentioned previously, there is no requirement that the sensitivity of each individual coil in an array be strictly sinusoidal, so long as the *net* sensitivity of the array is arranged to have the desired sinusoidal shape.

In a linear surface coil array with adjacent components, each coil j has a distinct but overlapping sensitivity $C_j(x, y)$. In the SMASH approach, signals from the various array components are combined with linear

weights, n_j, to produce overall composite sensitivity variations across the image plane of the form

$$C^{\mathrm{comp}}(x, y) = \sum_j n_j C_j(x, y) = \exp(im\Delta k_y y) \quad [4]$$

Here, m is an integer and $\Delta k_y = 2\pi/\mathrm{FOV}$, the minimum k-space interval corresponding to the desired field of view (FOV). In other words, the composite sensitivities are arranged to be spatial harmonics of the imaged field of view. By virtue of these sinusoidal spatial modulations, each combined data set is shifted in k-space by an amount $-m\Delta k_y$, as was outlined in the previous section

$$S(k_x, k_y) = \iint dx dy C^{\mathrm{comp}}(x, y)\rho(x, y) \exp\{-ik_x x - ik_y y\}$$

$$[5]$$

$$= \iint dx dy \rho(x, y) \exp\{-ik_x x - i(k_y - m\Delta k_y)y\}$$

$$= \hat{\rho}(k_x, k_y - m\Delta k_y)$$

If a total of M spatial harmonics are generated using linear combinations of component coil signals, then M lines of k-space may be reconstructed for each application of a phase-encoding gradient. The full-signal matrix may therefore be generated using a fraction $1/M$ of the usual phase-encoding gradient steps. Consequently, all the data for an image of a given resolution and field of view may be collected in a fraction $1/M$ of the usual acquisition time. (Since the linear combinations that yield distinct spatial harmonics are performed after the fact, they do not add in any way to acquisition time.) The k-space geometry of this acquisition strategy is illustrated in Fig. 1.

One advantage of the linear coil array design is that multiple spatial harmonics may be formed from the same simple set of component coils by using different linear combinations of the coil signals. Such an approach presumes that the necessary spatial harmonics may be faithfully represented by linear superpositions of component coil sensitivities. In fact, this is true for a wide range of component coil shapes and array geometries. Figure 2 demonstrates the situation schematically for a linear array of eight rectangular coils with slight overlap. Different weightings of the individual component coil sensitivities lead to net sensitivity profiles of different spatial frequencies. In Fig. 2, coil sensitivities (modeled schematically as Gaussian in shape) are combined to produce harmonics at various fractions of a fundamental spatial wavelength $\lambda_y = 2\pi/\Delta k_y$ which is on the order of the total array extent in y. The range of harmonics that may comfortably be generated in this way depends upon the width and spacing of the individual component coil sensitivity functions. Figure 2 demonstrates that, so long as the scale of the desired spatial variations is commensurate with the scale of the component coil sensitivities, harmonic generation is quite accurate. Five harmonics arising from the eight-coil array are represented in Fig. 2 (since complex combinations of the various sinusoids will yield complex exponentials with $m = -2, -1, 0, 1$, and 2). Simple algebraic considerations dictate that a
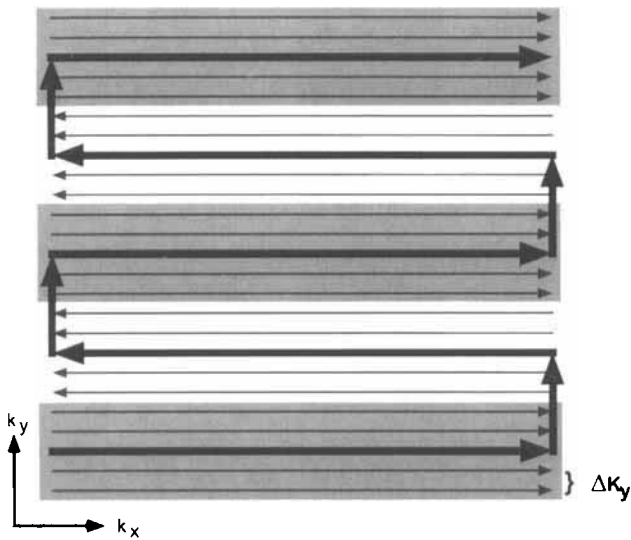
FIG. 1. Schematic k-space trajectory for a sample SMASH acquisition. Frequency-encoding gradient readouts are indicated by thick horizontal lines, phase-encoding gradient steps by thick vertical lines. Extra k-space lines derived from harmonics of the fundamental spatial frequency Δk_y are shown as thin lines. Here, five harmonics ($m\Delta k_y$, with $m = -2, -1, 0, 1$, and 2) have been used, for a total of five lines per readout (grouped by shading). This illustrative simultaneous acquisition procedure represents a five-fold savings in total acquisition time, as compared with a conventional acquisition with the same spatial resolution and FOV.
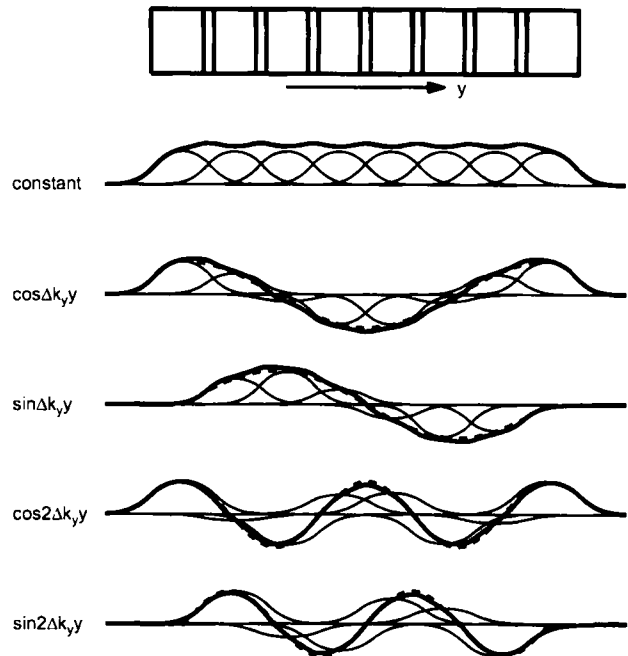

FIG. 2. Some possible linear combinations of component coil sensitivities for an example eight-coil phased array, approximating several spatial harmonics of frequency $m\Delta k_y$. Weighted individual coil sensitivity profiles are depicted as thin solid lines beneath each component coil. Dashed lines represent the sinusoidal or cosinusoidal weighting functions. Combined sensitivity profiles are indicated by thick solid lines. These combined profiles closely approximate ideal spatial harmonics across the array.

maximum of N linearly independent combinations may be formed from N component functions. In practice, due to the various geometrical constraints, the number of accurate harmonics will generally be less than the total number of array components.

Practical Considerations

Real-valued Gaussians were used to model the component coil sensitivities in Fig. 2. In actual practice, however, the sensitivity profiles of RF surface coils are represented not by simple Gaussians, but by more complicated functions which are complex-valued rather than purely real-valued. The coil sensitivity functions must describe both the magnitudes and the phases of the signals produced by precessing spins at various distances from the coil center, and the phases as well as the magnitudes vary with position and with coil geometry (14). In practical SMASH reconstructions, then, complex weights, n_j, must be used to account for the full content of the coil sensitivity functions. Alternatively, the phase variation in component coil sensitivities and images may be removed by taking absolute magnitudes, and the resulting real-valued sensitivities may be combined in the manner of Fig. 2.

Physically realizable coil arrays will also have spatial variations in directions other than the principal array direction. For linear surface coil arrays like that in Fig. 2, the shape of component coil sensitivity functions changes with distance from the coil, tending to widen and flatten with increasing distance. This means that it will generally be possible to synthesize higher frequency

harmonics close to the array than would be possible at a greater distance.

For oblique image slices tilted away from the principal array direction, sensitivity function widths will vary somewhat across the image, and spatial harmonic fits require a compromise between the various regions. Nevertheless, the regions in which component coil sensitivity functions are wide enough to interfere dramatically with spatial harmonic generation are generally regions of low overall sensitivity, which do not contribute substantially to the image intensity. Conventional phased-array images would also have low SNR in these regions.

In practice, therefore, the geometric constraints of spatial harmonic fitting are relatively forgiving. In numerical simulations as well as in actual image reconstructions, we have found the fitting procedure to be quite flexible for image FOVs spanning the length of at least several array components.

METHODS

Overview

We have implemented the principles outlined above in the following manner. First, linear RF coil arrays were selected with geometries suitable for spatial harmonic generation. The appropriateness of coil geometry was first tested in numerical simulations, using analytic integration of the Biot-Savart law to calculate the spatial variation in induced transverse magnetic fields, and

hence to determine the sensitivity profile of each coil. Taking into account the number of spatial harmonics that could comfortably be generated using the coil array, and therefore the fraction of the total k-space matrix to be collected, partial image acquisitions were planned and image data were acquired simultaneously in the separate channels of the array, using a fast imaging sequence. Since only a fraction of the usual signal data was to be used to generate the final images, only a fraction of the usual imaging time was spent on data collection.

Next, the individual coil image data were exported to a workstation for postprocessing. Individual complex sensitivity profiles were determined for each of the component coils in the array, using either phantom image data, *in vivo* image data, or numerical simulations. Optimal weights for linear combination of component coil signals were determined by iterative fitting of the sensitivity data to the target spatial harmonic sensitivity profiles, using a least squares fitting algorithm. The appropriate composite k-space-shifted signals were then formed, and the data sets interleaved, in the style Fig. 1, to yield the full k-space matrix, which was Fourier transformed to give the reconstructed SMASH image. Figure 3 is a pictorial summary of stages in the SMASH imaging procedure.

Materials

Images were obtained on two different commercial imaging systems, using a three-element and a four-element array. Materials, methods, and results from each of these arrays are presented in turn.

Three-Element Array

The raw data for images with the three-element array were generated on a commercial Philips NT 1.5 Tesla whole body clinical MR imager (Philips Medical Systems, Best, Netherlands). For the phantom images, a standard circular phantom of 200 mm diameter and varied internal structure was used. A prototype synergy coil manufactured by Philips was used as a SMASH coil array. The equivalent circuit for this coil consisted of three rectangular component coils arranged in a linear array with a slight overlap in the left-right direction, similar to the array shown schematically in Fig. 2. Fitting of spatial harmonics and image reconstruction were performed on an HP–735 UNIX workstation, and code for the postprocessing steps, as well as for supporting numerical simulations, was written in the Matlab programming environment (The Mathworks, Natick, MA).

Four-Element Array

The raw data for images with the four-element array were generated on a Siemens Vision 1.5 Tesla whole body clinical MR imager (Siemens Medical Systems, Erlangen, Germany), equipped with high performance EPI gradients (25 mT/m with 600 μs nonresonant rise times or 300 μs resonant rise times using an EPI booster). The commercial Siemens CP spine array coil was used for a four-element array. (The array actually contains six elements in total, of which four may be selected at any one time.) This coil is a linear array extending along the magnet bore in the foot-head direction. For postprocessing, the workstation and software described above for the three-element array were used.

Image Planning and Data Collection

Three-Element Array

Phantom Images. With the phantom centered over the coil array, data for the reference image were acquired in a 6-mm thick coronal slice parallel to and 80 mm above the plane of the array, using a TSE pulse sequence with five echoes per excitation. FOV was 200 × 200 mm (centered on the phantom), matrix size was 256 × 256, and phase encoding was performed in the left-right direction (i.e., in the direction of the coil array), with a single signal average. Data from each of the three component coil channels were acquired simultaneously and stored separately for later processing. Acquisition time was 10 s. Next, a second coronal slice using the same technique and imaging parameters was taken to serve as a measure of component coil sensitivity. It was acquired 12 mm above the first slice, in a region of uniform spin density in the phantom. Then, a third image at the same level as the first was obtained in half the time using twice the phase-encode step, and hence half the field of view, in the left-right direction. Matrix size was now 256 × 128. Acquisition time was 5 s, exactly half the time taken for the first image.

In Vivo Images. A healthy adult volunteer was positioned with his head above the coil array, and images were taken in the same plane and with the same parameters as for the phantom images, except that eight signal averages with a slice thickness of 10 mm were used to improve SNR. The coil sensitivity image from the phantom was also used as a sensitivity reference for the *in vivo* images.

Four-Element Array

Each of two adult male volunteers was positioned with the bottom four elements of the CP spine array centered in the region of the kidneys. The imaging sequence used for the first volunteer was a TSE sequence with a turbo factor of 9, matrix size 270 × 512, FOV 500 mm, slice thickness 8 mm, TE 32 ms, TR 700 ms. The image slice was tilted roughly 10° from the coronal toward the transverse plane to follow the lumbar and thoracic spine. Images of the second volunteer were taken in a purely coronal plane using a single-shot TSE sequence, with a total matrix size of 128 × 256. A centric-reordered phase encoding scheme was employed. FOV was 550 mm, slice thickness 8 mm, interecho spacing 4.2 ms. In both cases, phase encoding was performed in the foot-head direction, along the principal direction of the array. Acquisitions covering the full foot-head FOV (FOV 500 × 500 mm, matrix 270 × 512; FOV 550 × 550 mm, matrix 128 × 256) were stored as references. Half-time, half-FOV acquisitions (FOV 250 × 500 mm, matrix 135 × 512; FOV 275 × 550 mm, matrix 64 × 256) were stored for subsequent SMASH reconstruction.
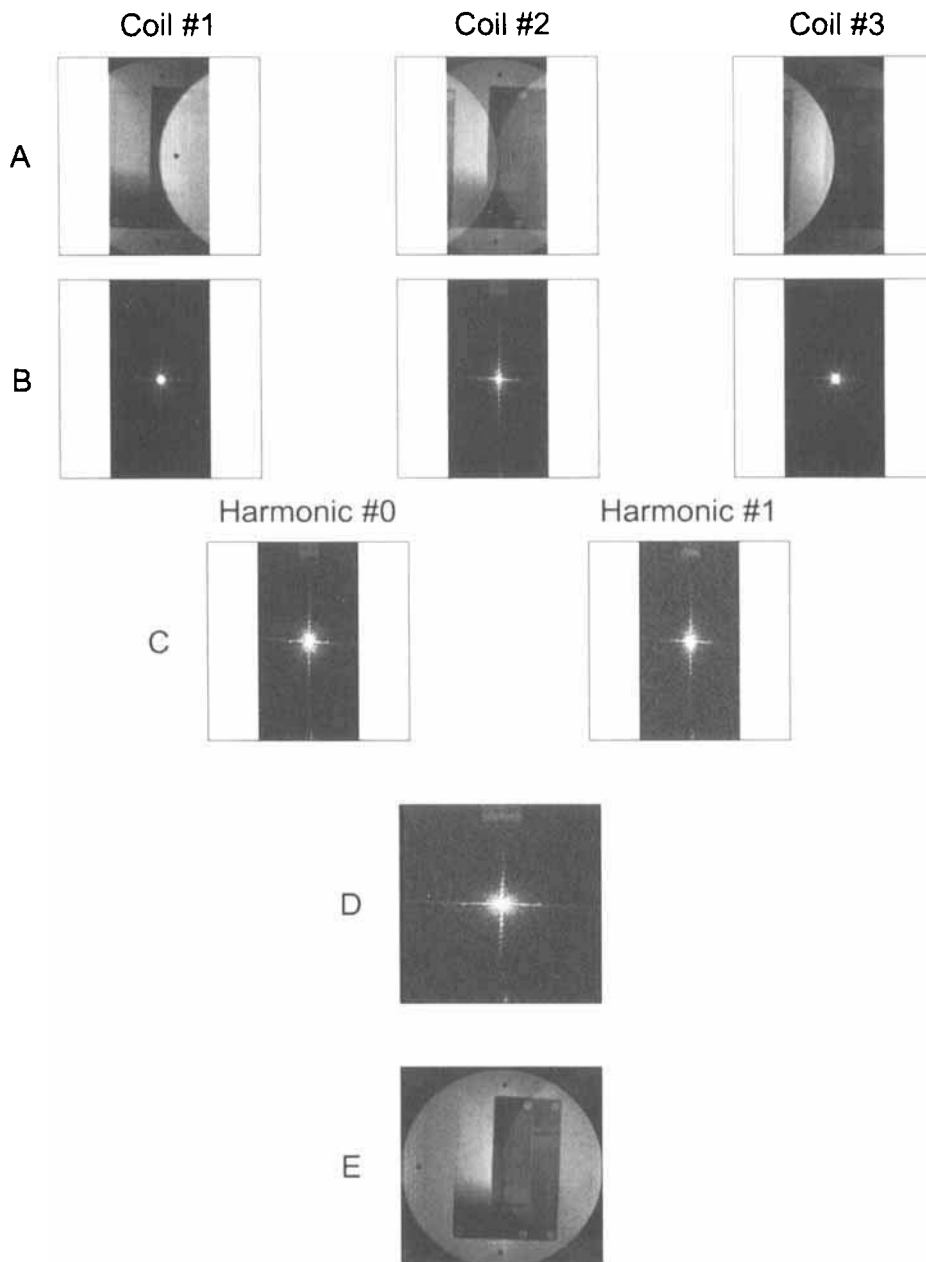
FIG. 3. Pictorial overview of the SMASH imaging procedure (depicting stages in the generation of the phantom image of Fig. 6b). (a) Aliased component coil images, corresponding to the half-time component coil signals in (b). (c) Weighted composite signals representing the zeroth (*left*) and first (*right*) spatial harmonics. (d) Full *k*-space matrix formed by interleaving the composite signals in (c). (e) Reconstructed image formed by Fourier transformation of the full signal matrix.

spans the entire extent of each image, and since the sensitivity reference image plane intersects the phantom in a region of uniform spin density, these intensity profiles correspond precisely to the complex sensitivity functions of the coils along the diameter. As expected, the sensitivity of each component surface coil falls off monotonically with distance from the coil. Note also the phase shift (betokened by the imaginary part of the sensitivity function) that grows with distance from the coil center. Using a gradient-descent fitting routine, these sensitivity functions were iteratively fitted to two target spatial harmonics: to the zero-frequency harmonic corresponding to uniform sensitivity, and to the first harmonic having a modulation wavelength equal to the FOV of 200 mm. Results of the fit are shown Fig. 5, which demonstrates that very close fits to the target harmonics may be achieved by component coil weighting, even with only three coils. These fits took roughly 15–20 s on our postprocessing workstation. Typical fitting times depend upon the criteria chosen for termination of the gradient-descent algorithm, and upon the available software and hardware, but we found that accurate fits could generally be accomplished in a matter of seconds.

Four-Element Array

In place of the phantom sensitivity reference used for the three-element array, an *in vivo* image of the first volunteer was used as a sensitivity reference for both volunteers. The four individual component-coil sensitivity reference images are shown in Fig. 4C. (These images were obtained in a coronal slice intersecting the center of the oblique slice used for reference and SMASH images in this volunteer. The imaging sequence was a FLASH sequence with *TE* 0.42 ms, *TR* 20 ms, flip angle 10°, matrix size 96 × 128, FOV 500 mm, slice thickness 8 mm. The short *TE* and *TR* were chosen to minimize tissue-specific relaxation contrast so that the

Determination of Coil Sensitivity and Optimal Component Coil Weights

Three-Element Array

First, sensitivity function data along the left-right diameter of the phantom was extracted from the component coil sensitivity reference images. The absolute magnitude images of coil sensitivity for each of the three component coils are displayed in Fig. 4A. Shown beneath them in Fig. 4B are the real and imaginary parts of the image intensity along a diameter. Since the phantom

Coil #1   Coil #2   Coil #3

A

B

- Real
- Imaginary

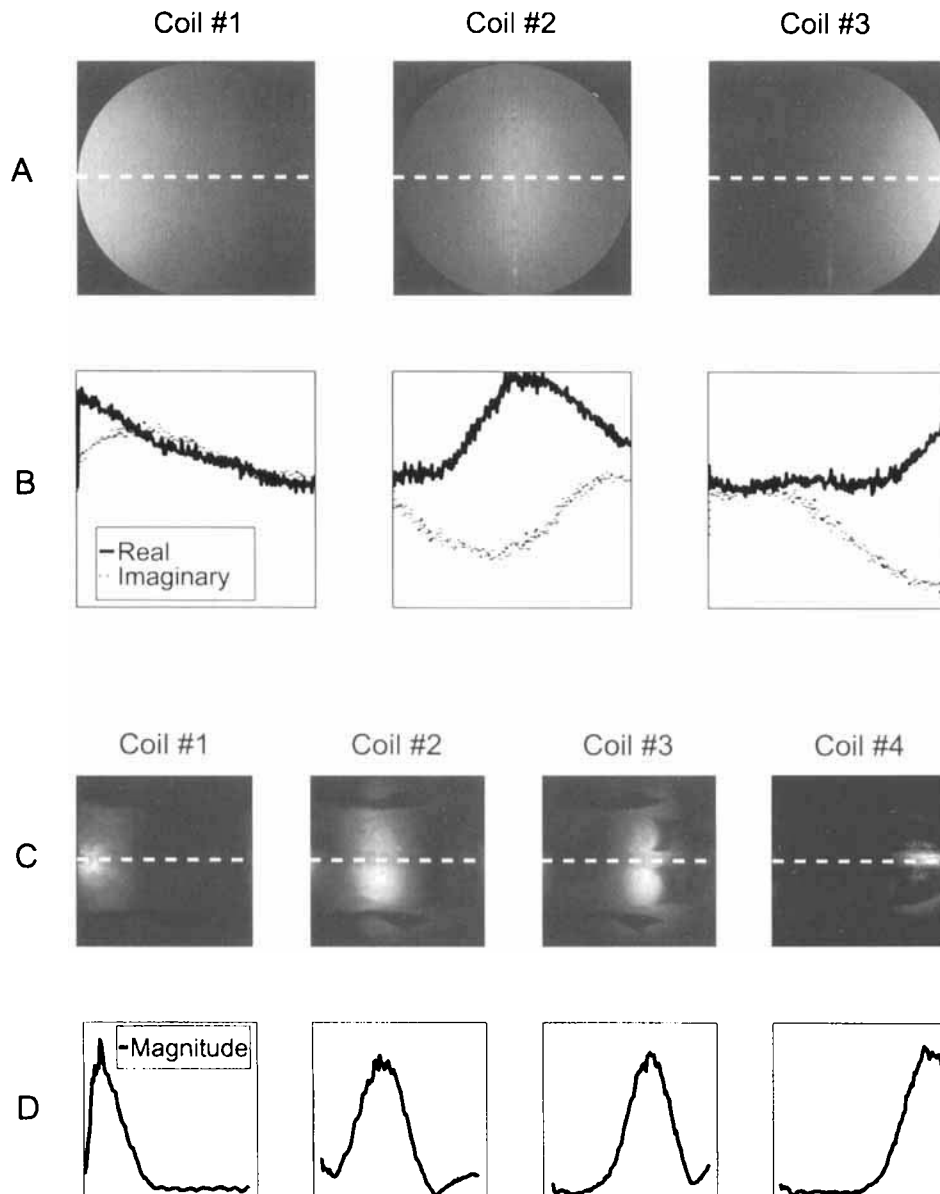## Coil #1   Coil #2   Coil #3   Coil #4

C

D

- Magnitude

FIG. 4. Component coil sensitivity information for the three-element and four-element arrays. (a,b) Sensitivity information for the three-element array, extracted from a phantom image slice with uniform spin density, and used to generate the SMASH images of Figs. 6 and 7. (a) Absolute magnitude images. (b) Sensitivity along the diameter indicated by dashed lines in (a). (c,d) *In vivo* sensitivity reference information used to generate the SMASH images of Figs. 8 and 9. (c) Absolute magnitude images of the abdomen and thorax of a healthy volunteer. For consistency, the images were transposed so that the foot-head phase encoding direction is horizontal. (d) Absolute magnitude sensitivity along the dashed lines in (c).

array is that absolute magnitudes of the sensitivity profiles were taken prior to fitting. This operation eliminates unwanted phase distortions due to field inhomogeneities, susceptibility artifacts, etc.

Image Reconstructions

Three-Element Array

Reference Images. The reference images in Figs. 6a and 7a were formed by Fourier transforming the three component coil reference signals and combining the resulting images pixel-by-pixel as the square root of the sum of square magnitudes.

SMASH Images. Figure 3 reviews various stages of SMASH reconstruction for the phantom image of Fig. 6b. (The procedure for the *in vivo* image of Fig. 7b was identical.) Using weights from the iterative fit, the three component coil signals (b) representing half-time, half-FOV aliased images (a) were combined into two composite data sets, one for the zeroth harmonic and one for the first harmonic (c). Finally, the two composite signal data sets were interleaved to form a data matrix of size 256 × 256 (d), and this matrix was Fourier transformed to yield the reconstructed image (e).

Four-Element Array

Reference images were reconstructed using the root-mean-square algorithm. SMASH reconstructions followed the scheme of Fig. 3, except that absolute magnitudes were taken of the component coil images in order to match the magnitude sensitivity references. The same set of weights from the spatial harmonic fit was used for both sets of images, despite the slightly different image planes and FOVs. For SNR estimation, the mean intensity in a region of nearly pure noise (boxed regions labeled N in the figures) was subtracted from the mean intensity of a region of relatively uniform signal (unlabeled boxed regions), and the difference was divided by the standard deviation of the

images would be as faithful as possible a representation of coil sensitivity.) Note that a single sensitivity reference in the general region of interest was used in order to test the flexibility of sensitivity reference measurement: No effort was made to obtain sensitivity information in the exact plane of the SMASH reconstructions.

With the sensitivity reference images in hand, intensity profiles along a central foot-head line following the spine were used to fit the zeroth and first spatial harmonics. These profiles are shown in Fig. 4D. One difference with the fitting procedure described above for the three-element
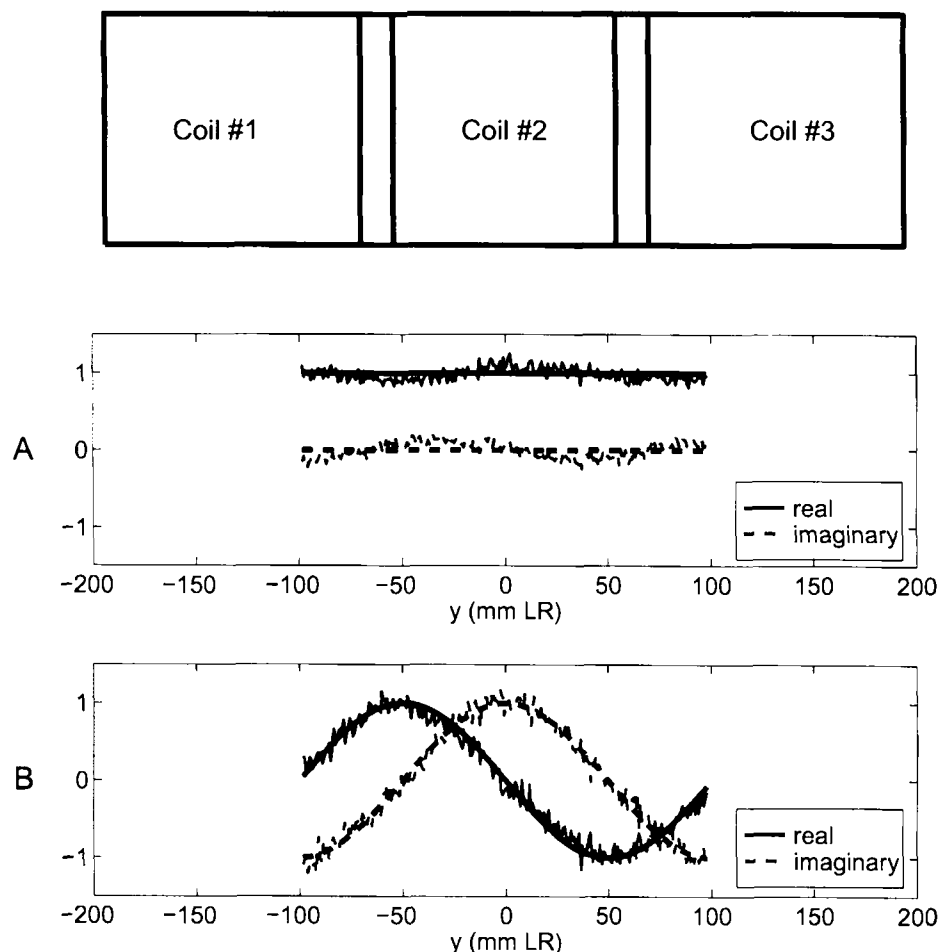
FIG. 5. Results of an iterative fit of spatial harmonics with weighted coil sensitivity functions. The three-element coil array is shown schematically on the same y scale as the spatial harmonic fits. (a) Best fit to homogeneous sensitivity (zeroth harmonic, $m = 0$). (b) Best fit to first harmonic ($m = 1$). Thick lines indicate target harmonic profiles (solid = real part, dashed = imaginary part); thinner jagged lines indicate weighted sensitivity data sets.

age of a healthy adult volunteer, acquired in 70 and 35 s, respectively.

Four-Element Array

Figures 8 and 9 show *in vivo* images obtained using the four-element phased array coil. Figure 8a contains a coronal TSE image of the abdomen and thorax of the first volunteer, acquired in the conventional manner in a 22-s breath-hold. The equivalent image acquired in 11 s using the SMASH technique is shown in Fig. 8b. Figure 9a shows a single-shot TSE image of the second volunteer, obtained in a conventional breath-hold acquisition of 540 ms. The SMASH image in Fig. 9b was acquired in 270 ms. Note that, as compared with images from the three-element array (Figs. 6 and 7), the images in Fig. 8 and Fig. 9 are almost entirely free of foldover artifact. Comparative SNR measurements have also been included in these two figures. The reference and the SMASH image of Fig. 8 have comparable SNRs of 40.4 and 39.2, respectively. In the regions measured in Fig. 9, the reference image SNR of 311.8 is even slightly exceeded by the SMASH image SNR of 327.5.

noise region intensity. This procedure is known to adjust to some extent for noise bias present in absolute magnitude images (15). While more exact procedures are known (16), they were not deemed necessary for the purpose of simple comparison. For each figure, the location and area of the regions interrogated in the conventional reference image were duplicated exactly for SNR measurement in the SMASH image.

RESULTS

Three-Element Array

The images in Figs. 6 and 7, respectively, demonstrate phantom and *in vivo* implementations of the SMASH imaging technique using the three-element phased array coil. Figure 6a shows the proton-density image of a water-filled phantom, obtained using the TSE sequence described previously, with a total conventional acquisition time of 10 s. Figure 6b shows the equivalent image obtained in 5 s with the SMASH technique.

Similar results are obtained *in vivo*. Figure 7 contains a conventional reference and a SMASH coronal brain im-

DISCUSSION

The acquisition speed of many of the existing sequential fast imaging sequences comes at some cost in spatial resolution or SNR. Low flip-angle sequences, for example, sacrifice overall signal strength in favor of short repetition times. By contrast, the SMASH-imaging technique allows a sequential imaging sequence of choice to be used to acquire the same data in a fraction of the usual time. Thus, SMASH shares all the limitations and advantages of the underlying sequential imaging sequences that are used to collect partial k-space information. As long as suitable spatial harmonics may be generated with a coil array, the additional acquisition time savings afforded by SMASH reconstruction involves no significant sacrifice in resolution or SNR.

Imaging Speed: SMASH for Fast and Ultrafast Imaging

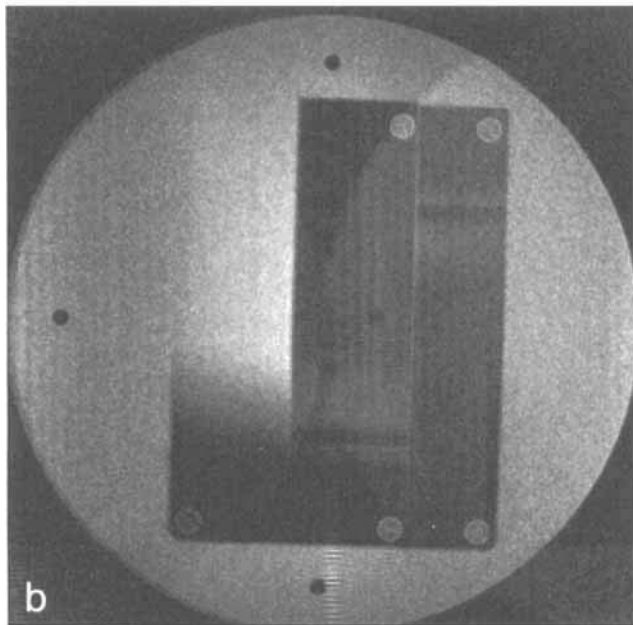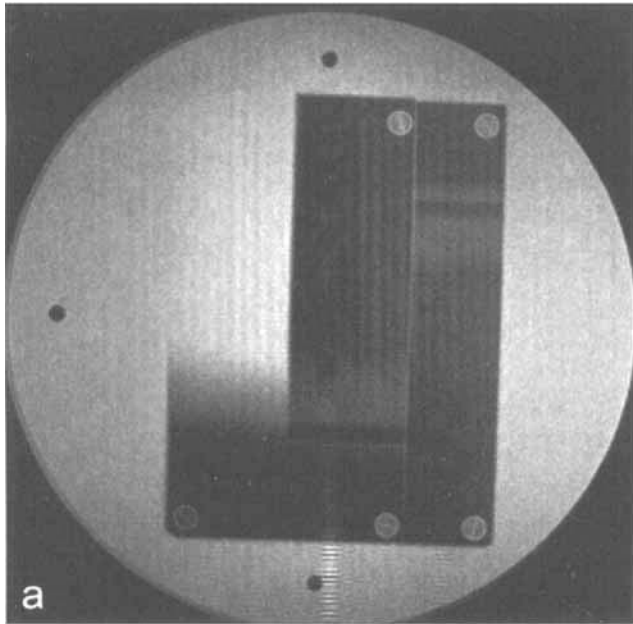To date, we have successfully implemented SMASH in combination with EPI, FLASH, HASTE, TSE, FISP, and

FIG. 6. Reference image versus SMASH image of a water-filled phantom, using a three-element phased array coil. (a) Reference image. Total acquisition time: 10 s. (b) SMASH image. Total acquisition time: 5 s. Phase encoding is in the left-right direction in both cases.
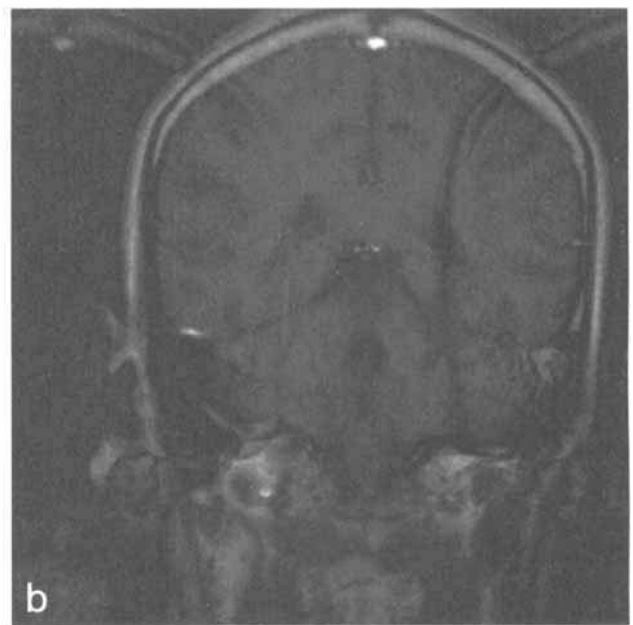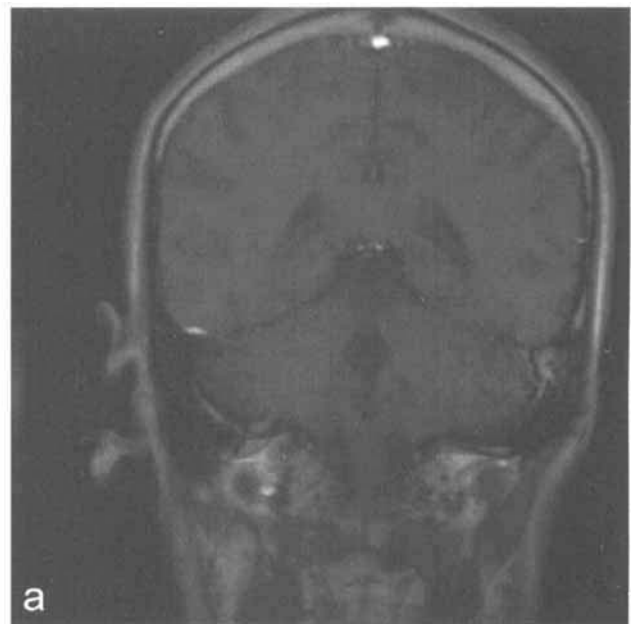
FIG. 7. *In vivo* reference image versus *in vivo* SMASH image of a healthy volunteer, using a three-element phased array coil. (a) Reference image. Total acquisition time: 70 s. (b) SMASH image. Total acquisition time: 35 s. Phase encoding is in the left-right direction.

segmented k-space gradient echo sequences. The images of Figs. 6–9 were included to demonstrate the methodology of SMASH imaging. These images themselves were not taken at the limits of achievable imaging speed. Nevertheless, SMASH has the potential to function as an ultrafast imaging strategy in that it may be used to multiply the intrinsic speed of the sequence with which it is used. If that underlying sequence is an ultrafast sequence such as EPI, then images may be acquired in a fraction of

the normal ultrafast-imaging time. The specific advantages of SMASH for single-shot imaging include a potential for increased SNR and/or decreased blurring artifacts due to diminished relaxation during a shortened acquisition time. As an example, in Fig. 9, the vertebral bodies appear sharper in the SMASH image (Fig. 9b) than in the corresponding conventional image (Figure 9a) as a result of decreased T_2 attenuation of high-frequency components in the shorter single-shot acquisition.
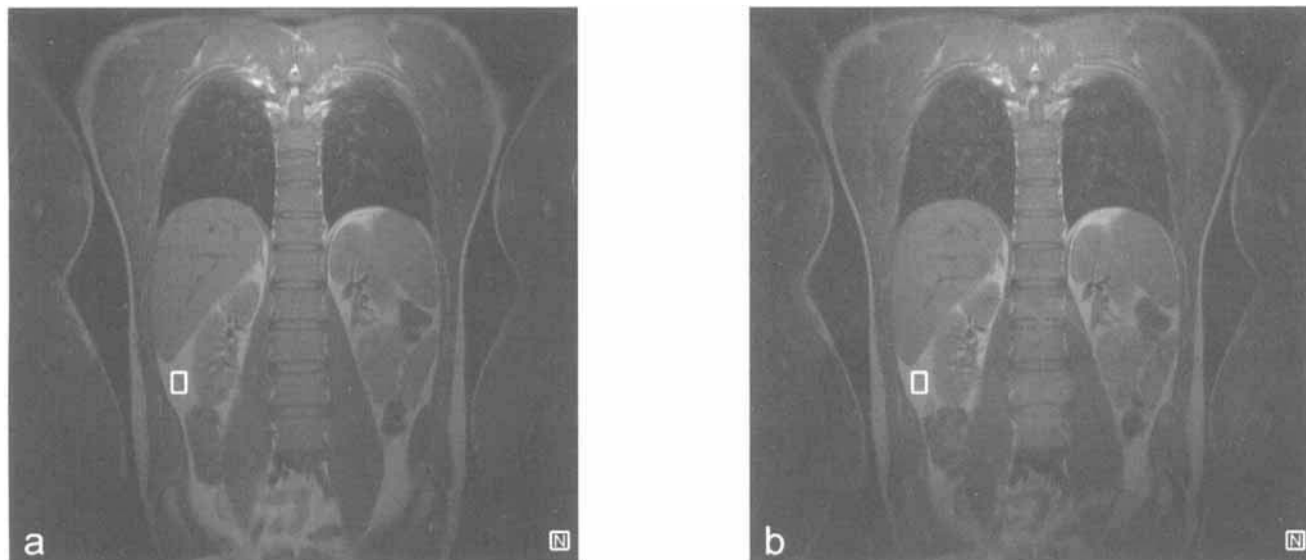
FIG. 8. Reference image versus SMASH image of a healthy adult volunteer, using a four-element phased array coil and a TSE imaging sequence. (a) Reference image. Total acquisition time: 22 s. SNR: 40.4. (b) SMASH image. Total acquisition time: 11 s. SNR: 39.2. Signal measurements were taken from the regions enclosed by an empty box, and noise estimates were taken from the boxed regions labeled with an N. Phase encoding is in the foot-head direction.

Reconstruction Speed: Postprocessing in SMASH

If sensitivity information appropriate to a given image slice is known in advance, then SMASH reconstruction involves only a set of simple weighted sums, followed by matrix reordering and a fast Fourier transform. In most of the cases presented here, SMASH reconstruction actually occurred *faster* than the conventional reference root-mean-square reconstruction of full-FOV images, despite the additional signal combination and k-space ordering steps involved in SMASH reconstruction. This is possi-

ble because individual FFTs of the various component coil images in the reference algorithm are replaced in SMASH by a single FFT of a combined data set.

Furthermore, the simple linear combinations involved in SMASH reconstruction are compatible with hardware-based as well as software-based approaches. In future implementations, SMASH reconstructions could be performed on the fly, eliminating even the small postprocessing time involved in SMASH image reconstructions, and leaving only the final FFT to software. This is one
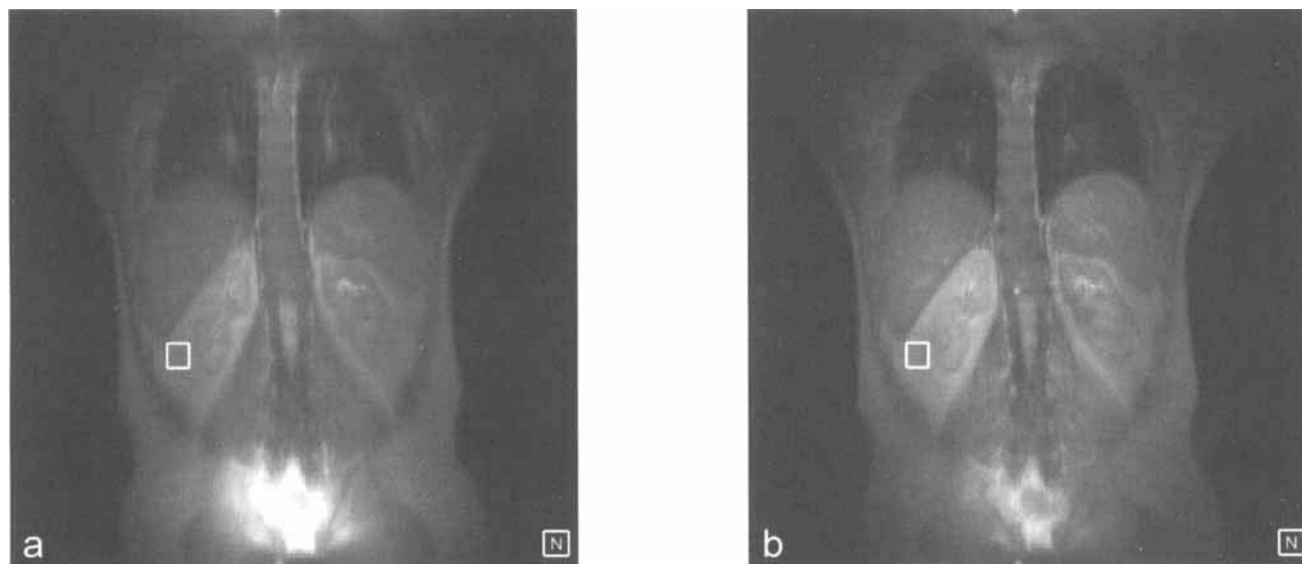

FIG. 9. Reference image versus SMASH image of another healthy volunteer, using a four-element phased array coil and a single-shot TSE imaging sequence. (a) Reference image. Total acquisition time: 540 ms. SNR: 311.8. (b) SMASH image. Total acquisition time: 270 ms. SNR: 327.5. As in Fig. 8, signal measurements were taken from the regions enclosed by an empty box, and noise estimates were taken from the boxed regions labeled with an N. Phase encoding is in the foot-head direction.

particular advantage of performing signal combinations in k-space rather than in the image domain.

Image Artifacts: Dependence on Component Coil Sensitivities

The greatest constraint of the SMASH imaging technique is its dependence on the measurement and manipulation of component coil sensitivities for spatial harmonic generation. Errors in spatial harmonics lead to aliasing artifacts, due to mismatch and mixing between the spatial frequency components of the image. Figures 6b and 7b both show evidence of such residual foldover artifacts. However, only faint vestiges of foldover artifact are visible in the lumbar spine region of the four-element SMASH images. The almost complete absence of aliasing artifacts in images taken with the four-element array indicates that these artifacts may be avoided in larger arrays with larger numbers of basis sensitivity functions available for harmonic generation. The image quality for a given time savings factor is expected to improve with number of array components, just as the maximum achievable time savings factor is expected to scale with element number.

As important as sensitivity reference estimation may be for SMASH imaging, it is also rather flexible. Sensitivity maps from phantom images were used for the SMASH reconstructions of Figs. 6 and 7, whereas direct *in vivo* sensitivity maps were used for the images of Figs. 8 and 9. A single set of weights derived from the *in vivo* sensitivity maps sufficed for accurate SMASH reconstruction in two different volunteers, and for two different slice positions, angulations, and FOVs. Numerical simulations of coil sensitivity may also be used, if these simulations have been reliably calibrated, and look-up tables may be constructed based on phantom images for multiple image planes. Other possibilities include low-pass-filtered versions of surface coil images (such as those that have been used for intensity correction in phased array imaging (17, 18)), or even image projections, such as those that may be obtained from the acquisition of a single line of k-space. Sequence-dependent effects of B_0 and B_1 magnetic field inhomogeneities may distort true coil sensitivities to some extent, but these effects may be addressed by direct fitting of absolute magnitudes, as was used in the reconstructions of Figs. 8 and 9. If magnitude fitting is not used in a sequence sensitive to field inhomogeneities, shimming should be performed, although a good weight-finding algorithm will be able to compensate for some degree of residual field inhomogeneity and generate accurate spatial harmonics, even in the presence of systematic phase or intensity errors. Finally, as discussed previously, the geometry of the coil array will place certain limitations on the FOV, position, and angulation of image planes suitable for SMASH reconstruction. Although a wide range of image plane geometries are compatible with SMASH reconstruction, the reconstruction may begin to fail at great distances from the component coils of the array. These constraints may be relaxed in the presence of increased numbers of component coils whose sensitivi-

ties provide good coverage of the imaging volume. Future work will involve the design of RF coil arrays specifically tailored for accurate and flexible spatial harmonic generation, which will help to overcome the limitations outlined here.

Signal-to-Noise Ratio

The SNR measurements in Figs. 8 and 9 show that SMASH reconstruction does not necessarily involve any sacrifice in SNR. SMASH uses linear combinations of signals from the components of a coil array, and thus shares the general advantages of phased array imaging: Localized surface coils have increased SNR as compared to larger coils, and the use of an array of surface coils provides increased SNR across the total extent of the array. Any SNR degradation in SMASH as compared with conventional phased array reconstruction will arise from noise correlations, since the same sets of component coil signals are combined in different ways to reconstruct multiple lines of k-space, and noise from each of the individual coils is replicated (albeit with different weights) in each of the different harmonic composite signals.

The absence of noise correlation effects in the measured SNRs of Figs. 8 and 9 may be understood by considering particular relations between the weights for different spatial harmonics. In general, the weights for spatial harmonic fitting show alternations that follow the target sinusoidal sensitivity variations. For example, the weights used to generate the schematic spatial harmonics in Fig. 2 were themselves orthogonal sinusoids, for which

$$\sum_j n_j^{(l)} n_j^{(m)} = 0. \qquad [6]$$

In other words, the vector dot product of the weights vanished for all harmonics with $l\Delta k_y \neq m\Delta k_y$. Since Fourier transformation is a linear operation, noise variances from individual signal points will add as a sum of squares. In SMASH, since different shifted signal points are synthesized from the same acquired set of signals, cross-terms between the differently synthesized signal points must be included in the sum. These cross-terms express the effects of noise correlations. If the input noise for all component coils has a similar statistical profile, then the cross-terms correspond to simple dot products of the weight vectors used to synthesize the different signal points. Thus, when the weight vectors are orthogonal, the cross-terms vanish, and there is no increase in effective noise variance due to noise correlations. For experimental coil arrangements like those used here, the orthogonality condition is approximately met, and SNR values like those in Figs. 8 and 9 may be achieved.

There is one noteworthy difference between the SNR profiles of the reference and the SMASH images presented here. The reference images were all generated using a sum-of-squares combination of component coil images, as described in Roemer *et al.* (19) and as has become a standard practice in phased-array imaging. This combination algorithm yields an essentially constant noise profile across the image, with varying signal

(and hence, varying SNR) that is enhanced in regions of significant overlap between component coil sensitivities. SMASH reconstruction, on the other hand, results in a constant-*signal* image with a varying noise profile. The linear combinations of component coil signals in SMASH are explicitly designed to produce a homogeneous composite signal. This is most obvious in the case of the zeroth harmonic combination, which produces a flat net sensitivity profile, C^{comp}, across the image plane (Fig. 5). Although the higher harmonics do involve significant spatial sensitivity variations, their profiles are all complex exponentials of unit modulus, and they do not lead to any intensity variations in the absolute magnitude image. (In other words, any apparent loss of sensitivity in the real channel is precisely compensated by a sensitivity gain in the imaginary channel.) SMASH reconstructions, therefore, do away with intensity peaks in regions of component coil overlap in favor of a spatially homogeneous image profile. In fact, sensitivity-dependent linear combinations may be used independently of SMASH as a method of homogeneity correction. A homogeneity-corrected version of the image in Fig. 6a may be generated by a linear combination of component coil reference images, using the weights calculated for the zeroth harmonic profile in Fig. 5. Roemer *et al.* (19) described an alternative combination algorithm for producing constant-signal images from phased arrays, and SMASH images produced with accurate spatial harmonics will have similar intensity profiles.

SMASH Imaging with Phased Arrays

The coil geometry pictured in Fig. 2 is essentially that of an MR-phased array coil (19–21). Indeed, many of the hardware components needed for SMASH imaging are present in traditional phased arrays, which contain multiple inductively decoupled coils with some spatial separation and separate receivers for independent data collection. Since their initial description, phased arrays have been used increasingly in many areas of clinical MR imaging. Nevertheless, with few exceptions, the bulk of phased-array applications to date have addressed increased *sensitivity*, with little effort toward improving image acquisition *speed*.

This distinction is essential in distinguishing SMASH imaging from conventional phased-array imaging. Whereas the conventional uses of phased arrays may be said to increase the SNR that can be achieved during a fixed acquisition time, they do not increase intrinsic acquisition speed. Despite the SNR advantages of phased arrays, a fixed region of *k*-space must still be traversed for each component coil in a conventional phased-array acquisition, and thus the total time required to acquire data of a given spatial resolution over a given FOV is still limited by the underlying imaging sequence. (For example, blurring due to physiological motion will be present in a phased array image just as much as in a single-coil image acquired using the same imaging sequence.) By contrast, SMASH allows images to be acquired in a fraction of the conventional sequence-dependent acquisition time, with the same SNR improvements as in conventional phased array images. Unlike in conventional

phased-array images, therefore, the time-dependent effects of physiological motion, spin relaxation, etc., will be reduced in SMASH images, since SMASH multiplies the intrinsic speed of any imaging sequence with which it is used.

Simultaneous Acquisition

Only a few proposals for simultaneous acquisition in MR have been described. Hutchinson and Raff in 1988 (8) proposed a theoretical simultaneous acquisition scheme in which all the data for an MR image would be collected in the course of a single echo using a multitude of very small pickup coils. Descriptions of a similar imaging technique, using inverse source procedures to reconstruct images from data collected in an array of coil detectors surrounding the imaged object, were published by Kwiat *et al.* (9, 10), who also built prototype detector arrays. Although these massively parallel techniques promise truly dramatic reductions in image acquisition times, their performance has yet to be established in actual practice. It is conceivable that the spatial harmonic reconstruction procedure of SMASH could be applied in coil arrays of the sort described by these investigators.

Carlson and Minemura (11) achieved a twofold acquisition time savings using two nested body coils. In their approach, partial data sets were collected simultaneously in the two coils, one of homogeneous sensitivity and the other with a linear gradient in sensitivity, and the missing lines in *k*-space were generated using a series expansion in terms of other phase-encoded lines. This approach to image reconstruction differs from the SMASH approach, although the net effect of both procedures is to use coil sensitivity information in place of some portion of the gradient phase encoding steps. Perhaps more importantly, the coils used by Carlson and Minemura were body coils, which provide greater volume coverage but significantly smaller overall sensitivity than surface coils, the properties of which are exploited in SMASH. To increase SMASH imaging speed beyond the twofold improvement already achieved, more surface coils can be added. Equivalent extensions of Carlson and Minemura's technique would be more complicated, since each increment in acquisition speed would require an additional body coil, which has a sensitivity profile distinct from that of the other coils and which is also substantially decoupled from all the other coils (a more delicate feat for body coils than for spatially separated surface coils).

Finally, Ra and Rim (12) described a simultaneous acquisition technique in which images of reduced FOV were acquired in multiple coils of an array and the Nyquist aliasing in those images was undone by reference to component coil sensitivity information. This unaliasing procedure involves a pixel-by-pixel matrix inversion to regenerate the full FOV from multiple copies of the aliased image data. In several respects, SMASH and the "subencoding" technique of Ra and Rim are similar. Both techniques rely on estimates of component coil sensitivities, whether in the form of stored data or of an appropriately chosen reference scan. Both techniques involve linear combinations of partial data sets to recon-

struct an image over the full field of view, and if the sensitivity data are stored in advance, roughly the same number of mathematical operations are required for reconstruction (although in a significantly different order). Artifacts due to imperfect reconstruction appear in both techniques in the form of residual aliasing.

There are at least two essential differences between SMASH and the subencoding procedure, however. First, in SMASH, a small number of distinct weights (namely, one per component coil per harmonic) is used for signal combinations, as opposed to a large number in the subencoding technique (i.e., a distinct weight for each pixel of each component coil image). The larger variety of weights in subencoding means that sensitivity variations at the single pixel level can be picked up in the reconstruction, but it also means that errors or artifacts present in the sensitivity references will be picked up pixel by pixel in the reconstructed image. SMASH, on the other hand, forces the number of distinct weights down to a small set by means of the spatial harmonic fitting procedure. This fitting process effects a partial smoothing of sensitivity data, in which anomalous points are discarded or assigned small importance. Furthermore, the set of weights in SMASH is fixed by the number of coils and harmonics, and is independent of image matrix size. This bypasses the need to acquire a new sensitivity reference or to interpolate from a stored reference when an image of a new matrix size is acquired.

The second major difference between SMASH and subencoding is that in SMASH, the combinations of component coil data occur in k-space prior to Fourier transformation. This fact, in combination with the small number of distinct weights in SMASH, make it particularly compatible with potential hardware implementations. Since each subencoding data set must be Fourier-transformed prior to reconstruction, acquisition must be completed before the necessary linear combinations can proceed. SMASH array signals, on the other hand, can be combined on the fly, point by point or echo by echo, yielding a fully reconstructed k-space matrix ready for Fourier transformation to an image as soon as acquisition is complete. This offers the prospect of replacing some of the digital postprocessing stages with operations in a small number of relatively simple hardware components, allowing for nearly instantaneous k-space reconstructions and for simple connections to existing receiver networks. Thus, the fact that SMASH signals are combined in k-space could provide practical advantages in future implementations.

CONCLUSION

The heart of the SMASH technique lies in a partial replacement of gradient phase encoding by a phase encoding procedure tied to the detection coils. In SMASH, the spatial modulations that distinguish different phase-encoding lines are generated by combining signals from multiple coils arrayed above or around the imaging volume. This shift of responsibility for phase encoding from gradient geometry to coil geometry, and from the spin preparation stage to the stage of signal detection and combination, allows for simultaneous acquisition of mul-

tiple lines of k-space. In this initial demonstration, a twofold acquisition time savings was achieved used existing technology, including coil arrays that were not optimized for SMASH imaging. With a suitable coil array, substantially larger factors may be expected.

Apart from its promise for progressively faster acquisitions, SMASH has a number of practical advantages as a fast-imaging scheme. As a partially parallel acquisition strategy, it can be combined with most existing sequential fast-imaging techniques for multiplicative time savings. No special hardware is required, other than an appropriate coil array. Commercially available MR-phased arrays may well suffice to yield significant time savings, and SMASH may be performed on machines not equipped with EPI gradient systems. Combinations of component coil signals are performed after the fact, allowing for a wide range of postprocessing steps, including fine tuning of spatial harmonics, adaptive artifact correction, or even nonFourier (e.g., wavelet) encoding and reconstruction. Spatial harmonic reconstructions automatically yield a homogeneous intensity profile for the reconstructed image. Of course, if acquisition speed is not a primary concern, SMASH coil arrays may also be used as standard phased arrays, simply by changing the data acquisition and reconstruction protocols without any changes in hardware. Finally, although recent studies have shown that the sensitivity advantages of phased arrays peak at coil numbers less than 6, the advantages of faster imaging with SMASH may provide an impetus for development of arrays with larger numbers of coils and with new coil geometries. It is apparent from Fig. 2, that the higher the frequency of the spatial harmonic desired, the larger the number of component coils required for its generation (since at least for simple component coil shapes, the sharpest features of the net sensitivity function can only be on the order of the component coil dimension). Even for a fixed acquisition speed, any extra sensitivity information from additional coils can be used for the fine tuning of spatial harmonics and the improvement of image quality.

The time gained in a SMASH acquisition may be used to collect extra data for better spatial resolution and/or SNR, or else faster acquisitions may be used to eliminate motion artifacts from mobile structures in the field of view. Of course, even in areas where image quality is not limited by spatial or temporal resolution, faster image acquisition will have the benefit of increasing the throughput of clinical MR machines, improving patient compliance during motion-sensitive procedures, and minimizing patient discomfort. The success of fast sequential-imaging sequences has raised the expectation that in time, the speed of MR imaging would fall below the threshold of the fastest physiological motions. A shift in strategy from serial to parallel MR acquisition promises to bring this goal to fruition.

ACKNOWLEDGMENTS

REFERENCES

1. P. Mansfield, Multi-planar image formation using NMR spin echoes. *J. Phys. C.* **10**, L55–58 (1977).

2. A. Haase, J. Frahm, D. Mattaei, W. Hanicke, K. D. Merboldt, FLASH imaging: rapid NMR imaging using low flip-angle pulses. *J. Magn. Reson.* **67**, 256–266 (1986).

3. J. Hennig, A. Nauerth, H. Friedburg, RARE imaging: a fast imaging method for clinical MR. *Magn. Reson. Med.* **3**, 823–833 (1986).

4. C. B. Ahn, C. Y. Rew, J. H. Kim, O. Nalcioglu, Z. H. Cho, A new high speed spiral-scan echo planar (SEPI) NMR imaging-I, *in* "Proc., SMRM, 4th Annual Meeting, 1985," p. 935.

5. C. B. Ahn, J. H. Kim, Z. H. Cho, *IEEE Trans. Med. Imaging* **MI-5(1)**, 2 (1986).

6. J. Hennig, M. Mueri, Fast imaging using burst excitation pulses, *in* "Proceedings, SMRM, 7th Annual Meeting, 1988," p. 238.

7. J. Hennig, M. Hodapp, Burst imaging. *MAGMA* **1**, 39–48 (1993).

8. M. Hutchinson, U. Raff, Fast MRI data acquisition using multiple detectors. *Magn. Reson. Med.* **6**, 87–91 (1988).

9. D. Kwiat, S. Einav, G. Navon, A decoupled coil detector array for fast image acquisition in magnetic resonance imaging. *Med. Phys.* **18**, 251–265 (1991).

10. D. Kwiat, S. Einav, Preliminary experimental evaluation of an inverse source imaging procedure using a decoupled coil detector array in magnetic resonance imaging. *Med. Eng. Phys.* **17**, 257–263 (1995).

11. J. W. Carlson, T. Minemura, Imaging time reduction through multiple receiver coil data acquisition and image reconstruction. *Magn. Reson. Med.* **29**, 681–688 (1993).

12. J. B. Ra, C. Y. Rim, Fast imaging method using multiple receiver coils with subencoding data set, *in* "Proceedings, SMRM, 10th Annual Meeting, 1991," p. 1240.

13. J. B. Ra, C. Y. Rim, Fast imaging using subencoding data sets from multiple detectors. *Magn. Reson. Med.* **30**, 142–145 (1993).

14. D. I. Hoult, R. E. Richards, The signal-to-noise ratio of the nuclear magnetic resonance experiment. *J. Magn. Reson.* **24**, 71–85 (1976).

15. D. C. Noll, D. G. Nishimura, Homodyne detection in magnetic resonance imaging. *IEEE Trans. Med. Imaging* **10**, 154–163 (1991).

16. H. Gudbjartsson, S. Patz, The rician distribution of noisy MRI data. *Magn. Reson. Med.* **34**, 910–914 (1995).

17. J. W. Murakami, C. E. Hayes, E. Weinberger, Intensity correction of phased-array surface coil images. *Magn. Reson. Med.* **35**, 585–590 (1996).

18. L. L. Wald, L. Carvajal, S. E. Moyher, S. J. Nelson, P. E. Grant, A. J. Barkovich, D. B. Vigneron. Phased array detectors and an automated intensity-correction algorithm for high-resolution MR imaging of the human brain. *Magn. Reson. Med.* **34**, 433–439 (1995).

19. P. B. Roemer, W. A. Edelstein, C. E. Hayes, S. P. Souza, O. M. Mueller, The NMR phased array. *Magn. Reson. Med.* **16**, 192–225 (1990).

20. C. E. Hayes, P. B. Roemer, Noise correlations in data simultaneously acquired from multiple surface coil arrays. *Magn. Reson. Med.* **16**, 181–191 (1990).

21. C. E. Hayes, N. Hattes, P. B. Roemer, Volume imaging with MR phased arrays. *Magn. Reson. Med.* **18**, 309–319 (1991).